

Original Research

Ecological Vulnerability of Tourism Scenic Spots: Based on Remote Sensing Ecological Index

Hui Shi¹, Tiange Shi^{1*}, Qin Liu², Zhi Wang²

¹Xinjiang University of Finance and Economics, No. 449 Beijing Road, Urumqi 830012, China

²State Key Laboratory of Desert and Oasis Ecology, University of Chinese Academy of Sciences, Beijing 100049, China

Received: 8 July 2020

Accepted: 2 November 2020

Abstract

The assessment of ecological vulnerability plays an important role in the protection and management of scenic tourism sites. In this study, using remote sensing image data in the same month of 2000 and 2017, ecological vulnerability in the Tianchi Scenic Area (TSA) was analyzed by calculating the remote sensing ecological index (RSEI), and the influencing factors of ecological vulnerability were detected using the geographical detector model. From 2000 to 2017, the values of wetness, dryness, and temperature in the study area increased, and the value of greenness and RSEI decreased. Spatial correlations of the RSEI were significant, showing strong spatial agglomeration and alternating cold spots-hot spots-cold spots-hot spots from north to south. The impact factors of land use type, temperature, and precipitation showed greater contribution to ecological vulnerability. In addition, the local government implemented policies such as prohibition of mining, grazing prohibition, and landscape protection, which decreased ecological vulnerability in the study area. This study provides a reference for the formulation of ecological vulnerability protection measures in the TSA and theoretical basis for defining the monitoring indicators for heritage sites around the world.

Keywords: remote sensing ecological index, spatial-temporal characteristics, influence factors, tourism scenic spots, vegetation diversity

Introduction

Global change and the intensification of human activity have a significant impact on the ecosystems [1]. With the increasing concerns on the global environmental change, ecological fragile belts and ecological vulnerability and its impact factors have become global research topics [2, 3]. Ecological vulnerability assessments and spatial correlations

reveal the spatial and temporal characteristics of regional ecological vulnerability and have important practical significance for ecological and environmental protection, rational use of resources, and sustainable development [2, 4]. Therefore, ecological vulnerability has become one of the most important topics in the study of global environmental change and sustainable development [5, 6].

Ecological vulnerability stems from the concept of “ecological transition zone” proposed by American ecologists in the early 20th century [7]. There is still some controversy about the concept of ecological vulnerability, but vulnerability is commonly used

*e-mail: stg@xjufe.edu.cn

to characterize the ecosystem's response to external pressure [8, 9]. The Intergovernmental Panel on Climate Change (IPCC) defines it as the system's sensitivity to external pressure. It can be characterized in three aspects: 1) external pressure on the ecosystem; 2) the sensitivity of the ecosystem; 3) the adaptability or elasticity of the ecosystem [10, 11]. Ecological vulnerability refers to the sensitivity and resilience of an ecosystem under the disturbance of external factors at a specific time and space scale, which is determined by its own attributes and external human factors [12]. Research on ecological vulnerability assessment has passed through the stages of the qualitative assessment of early vulnerability zone division and theoretical discussion, quantitative assessment, and system vulnerability discussion [13]. At present, there are many evaluation systems for ecological vulnerability, but a set of recognized models has not been formed, and evaluation indicators and calculation methods are not unified [14]. Commonly used conceptual models include the ecological sensitivity, resilience, and pressure degree (SRP) model [15], exposure, sensitivity, adaptability (VSD) model [16] and the pressure, sensitivity, elasticity (PSE) model. The indicator system includes the systems of natural causes-result performance, influencing factors-performance factors-stress factors, and the natural-ecological-socioeconomic system [17]. Evaluation methods include the analytic hierarchy process (AHP) method [18], comprehensive index method [19], fuzzy mathematics method [20], principal component analysis (PCA) method [21], neural network method [22], entropy weight method [6], the method of landscape ecology [23], and the fuzzy matter-element evaluation method [2].

With the development of the "3S" technology, remote sensing (RS) methods have been increasingly used in ecological vulnerability research due to their rapid, real-time, and multi-scale monitoring capabilities [24-26]. To select appropriate monitoring indicators, ecological vulnerability has been evaluated for a single indicator or multiple indicators [27]. Comprehensive evaluation models with multiple indicators include an ecological and environmental assessment model composed entirely of remote sensing data and a comprehensive index model composed of multiple indices using AHP [28, 29]. The comprehensive assessment model of ecological vulnerability composed of remote sensing data can reflect the vulnerability characteristics of the ecological environment in a timely, rapid, and objective manner [30]. Xu (2013) proposed a remote sensing ecological index (RSEI) by integrating various indicators such as greenness, humidity, heat, and dryness with remote sensing information [31]. The indicators of the RSEI are determined by the nature of the remote sensing data. The calculation method of RSEI not only reduces the influence of human subjective factors in actual operation, but also realizes high-precision visual expression of ecological vulnerability results in time and space [32]. It has the advantages of objectivity,

multiple indicators, and a wide range, which offsets the deficiencies of the existing technology, reduces the difficulty of extracting ecological indicators, and avoids the subjectivity in practical applications [33, 34]. Therefore, the RSEI can be used to objectively calculate ecological vulnerability and rapidly analyze its spatial distribution characteristics [35].

The ecological environment is fragile in the arid region of Northwest China and highly sensitive to global climate change [29]. The Xinjiang Tianshan Heritage Site consists of four districts, Tormur, Bogda, Kalajun-Kuerdening, and Bayanbulak. The Tianchi Scenic Area (TSA) is an important part of the Bogda Heritage Area, whose vertical natural zones directly affect the biodiversity and ecological succession process and objectively reflect the community function and structure. Since the successful declaration of the Tianshan Heritage Site in Xinjiang, the TSA has become a popular tourist destination [36]. From 2000 to 2017, the number of tourists increased from 421,200 to 2,095,600. However, tourism activities, infrastructure, and construction of new roads pose a threat to the ecological and environmental protection efforts [37]. Previous studies on the conservation of the ecological environment in the TSA investigated the impact of climate change on the ecological environment in the scenic area, the impact of grass cover and rain intensity on runoff, key technologies for geological disasters and ecological environmental protection, the extraction method for the vertical natural band spectrum, the evaluation of lake ecosystem services, spatial differentiation of ecological security and driving mechanisms, geological and ecological risk assessment, and soil characteristics and their environmental significance near the scenic roads [19, 37-45]. However, there are only a few studies that investigated the ecological vulnerability and its influencing factors through remote sensing. Previous studies on ecological risk and ecological security in the study area, mostly use comprehensive multi-factor evaluation methods. In this method, the factors are carried out by experts, thus making the results subjective. This study refers to Xu Hanqiu's ecological risk remote sensing calculation method, it can objectively and truly reflect the risk situation suffered by the ecosystem of the heritage site [46]. Through the discussion of the factors to ecological vulnerability, the strengthening of heritage ecosystem management and regional security has important practical significance and provides a theoretical basis for the subsequent implementation of the protection, monitoring and management policies of heritage sites [47].

In this study, ecological vulnerability of the TSA was calculated using the RSEI based on TM and OLI data, the temporal and spatial distribution of the ecological vulnerability was analyzed, and the influencing factors were detected using the geographical detectors model. The goal was to investigate the temporal and spatial evolution of ecological vulnerability and provide

the decision-makers with a theoretical basis for the protection and management of ecological vulnerability in the study area.

Materials and Methods

Study Area

The TSA is located in Fukang City, Changji Prefecture, Xinjiang, China, at the geographic coordinates of 88°0'38"-88°25'51"E, 43°44'53"-44°4'55"N. The study area is about 100 kilometers away from Urumqi, the capital of Xinjiang Uygur Autonomous Region in China. The total area is 548 km², and the tourist area is 28 km², accounting for 5% of the total area. The elevation gradually increases from north to south, from 1380 to 5445 m. The TSA is located in an arid area, which belongs to a continental temperate climate zone. The climate is warm in winter and cool in summer, with long hours of sunlight, and deep snow cover. The average annual temperature is 2.55 °C, and the relative humidity is 70-85%. The average annual precipitation is 443.9 mm, and it is concentrated from April to September. The average annual evaporation is 1439 mm [41]. The TSA covers 68.27% of the Bogda Heritage Site. There is a typical vertical mountainous natural belt on the northern slope of the Xinjiang Tianshan Mountain [36, 42].

These vertical mountainous natural belts are typical in temperate arid regions of the world. The TSA has six distinct vertical natural belts, which are distributed as a temperate desert belt (700-1,100 m), mountain steppe belt (1,100-1,650 m), mountain coniferous forest belt (1,650-2,700 m), subalpine-alpine meadow belt (2,700-3,300m), alpine cushion vegetation belt (3,300-3,700 m), and snow belt (3,700-5,445 m) [48]. The site was rated as a 5A scenic spot in 2007 and was one of the first scenic spots in the country to be included in the national scenic spots in 1980 (Fig. 1).

Data Source and Pre-Processing

The data required for this study include the digital elevation model (DEM) data, remote sensing data, land use type data, and field data.

DEM data. Through the geospatial data cloud website, the DEM data with a resolution of 30 m were downloaded. The resolution of the DEM data is consistent with the remote sensing data. Using ArcGIS 10.5 software, the range of the TSA area and the DEM data were superimposed to obtain the DEM data of the study area.

Remote sensing data. The remote sensing data were obtained from Landsat 5 TM on June 13, 2000 and Landsat 8 OLI_TIRS on June 4, 2017. The requirements for image selection criteria were as follows: the cloud cover should be less than 5%, and the seasonal

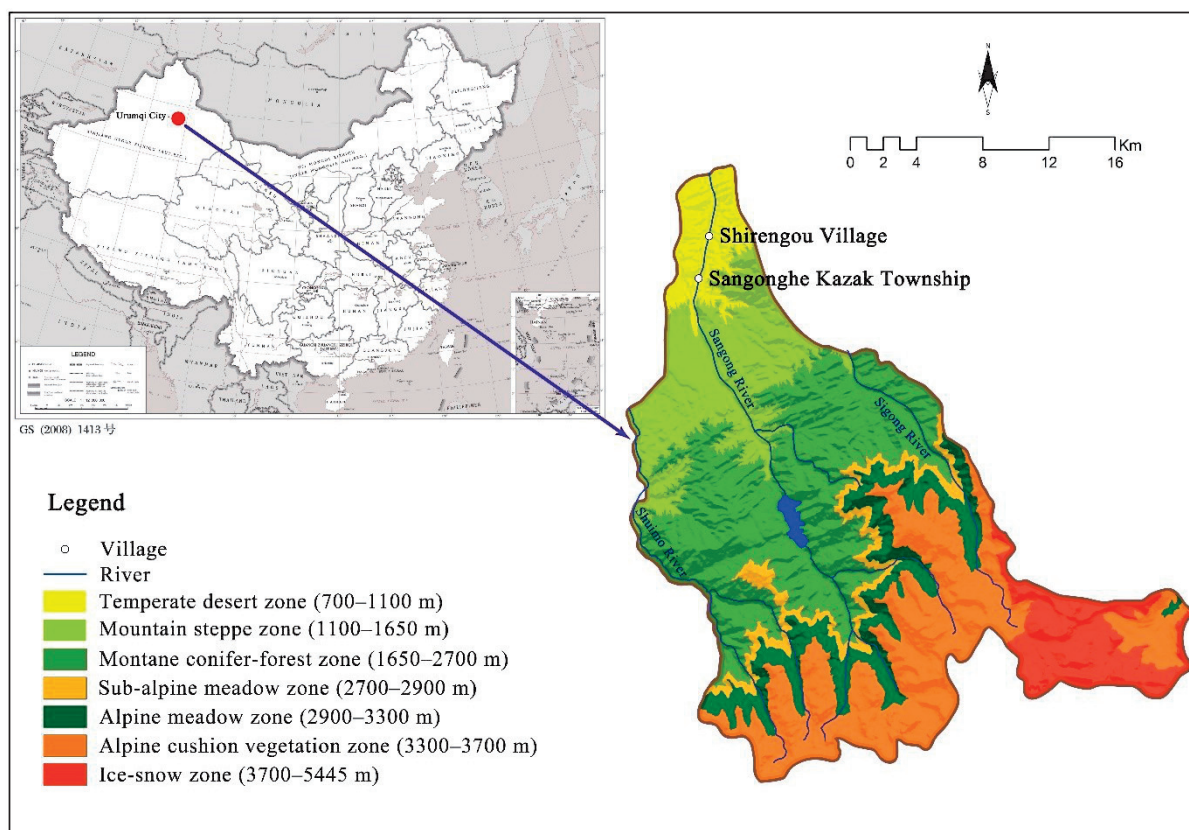


Fig. 1. Location and natural vertical belts of the Tianchi Tourism Scenic Spots.

differences should be small. The remote sensing data were obtained from the geospatial data cloud website. The ENVI 5.3 software was used to perform band fusion, radiation calibration, atmospheric correction, and geometric correction on two phases of remote sensing data. Then, the processed data were cropped based on the boundary of the study area.

Land use type data. Combined with China’s land use classification standards and field surveys, the land use types were divided into the bare-rock area, glaciers, water bodies, low-coverage meadow, medium-coverage meadow, high-coverage meadow, forest, agricultural area, and construction area, using the two phases of remote sensing data. In remote sensing data interpretation, first, an interpretation mark was established through Google Earth images and field survey data. Second, ENVI 5.3 software was used with the support vector machine classification method for remote sensing data interpretation through human-computer interactions. Finally, the accuracy of the interpretation results was verified using the high-resolution remote sensing images and the field survey data. In 2000 (2017), the land use classification accuracy was 85.03% (88.21%), and the Kappa coefficient was 0.857 (0.873).

Field data. To verify the consistency of the results with the real-world data, we collected a total of 58 plots in 2018-2019 (July, vegetable growth season) to conduct vegetation surveys in the TSA. For the plot selection, the altitude, topography, soil conditions, and vegetation types in the same conditions should not be very different. The size of the plots was 10 m × 10 m. Three sets of repetitions were required. In a selected plot, the size of the herb plot was set to 1 m × 1 m, and the measurements were repeated in five groups. The data of the vegetation species name, height, coverage, number of plants, and crown width in each sample were recorded, and then the Simpson index, Shannon-Wiener diversity index, and Margalef richness index were calculated.

Methodology

Framework of Ecological Vulnerability in TSA

The ecological vulnerability was assessed using the remote sensing ecological index in this study [49, 50]. Then, the spatial-temporal evolution characteristics of ecological vulnerability were analyzed at different time periods using the exploratory spatial data analysis

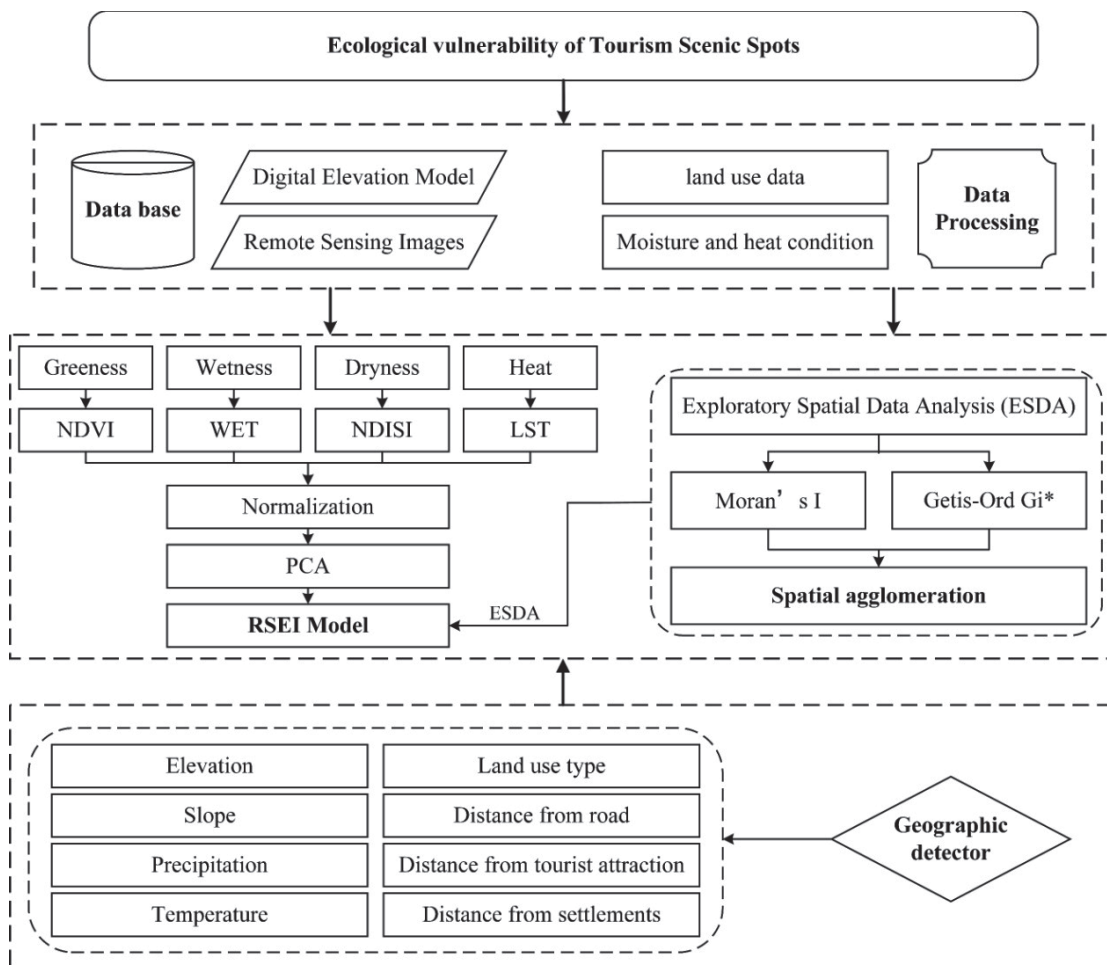


Fig. 2. Framework of ecological vulnerability in study area.

(ESDA) model [51]. Using the geographical detectors model, the influencing factors and the temporal and spatial evolution mechanism of ecological vulnerability were determined. The framework of ecological vulnerability consists of four parts. (1) Data collection and processing: The database, which contained the DEM data, remote sensing data, land use type data, and field survey data, was established. (2) Evaluation of ecological vulnerability: referring to the research of Xu (2013), the RSEI was used to assess the ecological vulnerability in the study area. The RSEI contains the indicators of greenness, wetness, dryness and heat, which are represented by Normalized difference vegetation index (NDVI), Wetness (WET), Dryness (NDISI), and Heat (LST) index, respectively [34, 52]. Then, the indicators of NDVI, WET, NDISI, and LST were analyzed using the principal component analysis (PCA) method to establish the RSEI [31, 53]. (3) Spatio-temporal characteristics: Using the ESDA model, spatio-temporal characteristics of ecological vulnerability were analyzed in 2000 and 2017. (4) Influencing factors: Based on the previous research, the influencing factors were analyzed through the geographical detectors model of the study area in 2000 and 2017 [54] (Fig. 2).

Comprehensive Assessment Model of Ecological Vulnerability

The RSEI is a new type of remote sensing index used to reflect the status of the regional ecological environment. With the indicators of greenness, humidity, dryness, and heat, the RSEI was used to comprehensively reflect the ecological vulnerability. The indicators of greenness, wetness, dryness, and heat are represented by NDVI, WET, NDISI, and LST index, respectively [49, 55].

(1) Indicators of RSEI

– Greenness

Vegetation is an important factor reflecting the regional ecological environment. Normalized difference vegetation index (NDVI) is the most widely used vegetation index to detect vegetation coverage, plant growth, and leaf area index [56, 57]. The NDVI is calculated as follows:

$$NDVI = \frac{b_{NIR} - b_{Red}}{b_{NIR} + b_{Red}} \tag{1}$$

...where NDVI is the index of greenness; b_{Red} and b_{NIR} denote the planetary reflectance of the red and near-infrared band of the Landsat 5 TM and Landsat 8 OLI images, respectively.

– Wetness

Wetness reflects the moisture of soil, vegetation, and surface water in the ecological environment. Brightness, greenness, and wetness obtained by remote sensing tassle cap transformation are widely used in ecological environment monitoring research [58, 59]. Based on

the data of Landsat 5 TM and Landsat 8 OLI images, wetness can be calculated as follows:

$$Wet_{OLI} = 0.1511b_{Blue} + 0.1972b_{Green} + 0.3283b_{Red} + 0.3407b_{NIR} - 0.7117b_{SWIR1} - 0.4559b_{SWIR2} \tag{2}$$

$$Wet_{TM} = 0.0135b_{Blue} + 0.2021b_{Green} + 0.3102b_{Red} + 0.1595b_{NIR} - 0.6806b_{SWIR1} - 0.6109b_{SWIR2} \tag{3}$$

...where b_{Blue} , b_{Green} , b_{Red} , b_{NIR} , b_{SWIR1} , and b_{SWIR2} are the planetary reflectance values of the blue, green, red, near-infrared, and mid-infrared bands of the Landsat 5 TM or Landsat 8 OLI images, respectively.

– Dryness

The dryness of the surface is caused by vegetation removal and construction activities. According to the land use classification of the study area, the bare soil index and the building index were selected to synthesize the dryness index and to calculate the environmental dryness of the area [29].

$$IBI = \left\{ 2 * \frac{b_{SWIR1}}{(b_{SWIR1} + b_{NIR})} - \left[\frac{b_{NIR}}{(b_{NIR} + b_{Red})} + \frac{b_{Green}}{(b_{Green} + b_{SWIR1})} \right] \right\} \left\{ 2 * \frac{b_{SWIR1}}{(b_{SWIR1} + b_{NIR})} + \left[\frac{b_{NIR}}{(b_{NIR} + b_{Red})} + \frac{b_{Green}}{(b_{Green} + b_{SWIR1})} \right] \right\} \tag{4}$$

$$SI = \frac{[(b_{SWIR1} + b_{Red}) - (b_{Blue} + b_{NIR})]}{[(b_{SWIR1} + b_{Red}) + (b_{Blue} + b_{NIR})]} \tag{5}$$

$$NDISI = \frac{IBI + SI}{2} \tag{6}$$

...where IBI is the bare soil index, SI is the building index, NDISI is the index of dryness.

– Heat

As an important indicator of environmental analysis, surface temperature is closely related to vegetation and water resources in the environment [60, 61]. In this study, the land surface temperature represents the heat index, which can be calculated as follows:

$$L_\lambda = gain * DN + bias \tag{7}$$

$$T_b = \frac{K_2}{\ln\left(\frac{K_1}{L_\lambda} + 1\right)} \tag{8}$$

$$LST = \frac{T_b}{\left[1 + \left(\frac{\lambda T_b}{\rho}\right) \ln \varepsilon\right]} \tag{9}$$

...where L_λ is the radiance value of the Landsat 5 TM thermal infrared 6 band and Landsat 8 OLI thermal infrared 10 band. T_b is the at-satellite brightness temperature, and K_1 and K_2 are the thermal conversion constants. LST is the heat index, DN is the pixel value of

the Landsat 5 TM thermal infrared 6 band and Landsat 8 OLI thermal infrared 10 band. Values of gain and bias can be obtained from the header file of the image. At the thermal infrared band of Landsat 5, $K_1 = 607.76W/(m^2 \cdot sr \cdot \mu m)$ and $K_2 = 1260.56K$; at the thermal infrared band of Landsat 8, $K_1 = 774.89W/(m^2 \cdot sr \cdot \mu m)$ and $K_2 = 1321.08K$. λ is the wavelength of the thermal infrared band; $\rho = 1.4380 \cdot 10^4 \mu m$; ϵ is the surface specific emissivity.

(2) Construction of RSEI

The PCA method can remove the correlation between various indicators by rotating the spatial coordinate axis of the characteristic spectrum, thereby concentrating the information to fewer principal components. When the cumulative variance contribution rate of a component is greater than or equal to 85%, that component represents the majority of relevant information. This method is widely used in the construction of the RSEI [62]. Its biggest advantage is that the weight value of the integrated indicators is not artificially determined but is objectively determined according to the nature of each indicator and its contribution to each principal component. Therefore, it avoids the deviations in the results caused by different weights set by people, making the RSEI more objective and reliable [63].

Due to the different dimensions of the indicators, the NDVI, WET, NDISI, and LST should be standardized to the values within [0,1] before the principal component transformation to reduce the impact of the time differences. According to the contribution to the RSEI, NDISI and LST are positive indicators, and NDVI and WET are reverse indicators. The standardization of the indicators adopts the range standardization method [25, 46].

$$SI_i = \frac{[I_i - I_{min}]}{[I_{max} - I_{min}]} \quad (10)$$

$$SI_i = \frac{[I_{max} - I_i]}{[I_{max} - I_{min}]} \quad (11)$$

...where SI_i represents the standardized value of the i -th index, ranging between 0 and 1; I_i is the actual value of the i -th index; I_{max} is the maximum value of the i -th index; I_{min} is the minimum value of the i -th index.

Using the ENVI 5.3 software, the standardized NDVI, WET, NDISI, and LST indicators were analyzed with the PCA method to calculate the RSEI, which represents ecological vulnerability of the study area [30].

$$RSEI = PCA[f(DVI, WET, NDISI, LST)] \quad (12)$$

...where RSEI represents ecological vulnerability. PCA is the method of principal component analysis. To facilitate the measurement and comparison of indicators, the RSEI was normalized to a value between 0 and 1.

Based on the RSEI value, the natural classification method was used to determine the classification of

ecological vulnerability, in which grades I–V indicate the ecological vulnerability from low to high.

Spatial Statistical Model

(1) Exploratory spatial data analysis (ESDA)

Exploratory spatial data analysis (ESDA) measures the spatial agglomeration degree. By calculating the spatial autocorrelation coefficient, ESDA describes the spatial agglomeration and anomaly of the spatial distribution patterns of visual objects to discover the spatial interactions between the objects [51, 64]. The ESDA model has two analysis methods: global statistics and local statistics.

– Global spatial autocorrelation

The global spatial autocorrelation is an overall quantitative description of the observed spatial patterns and used to detect the spatial correlation pattern of the entire study area [65].

$$\text{Moran's } I = \frac{N \sum_{i=1}^n \sum_{j=1}^n W_{ij} (x_i - \bar{x})(x_j - \bar{x})}{\sum_{i=1}^n (x_i - \bar{x})^2 (\sum_{i=1}^n \sum_{j=1}^n W_{ij})} \quad (i \neq j) \quad (13)$$

...where Moran's I is the index of the global spatial autocorrelation; N is the total number of raster data center points, with the size of $30 \text{ m} \times 30 \text{ m}$ in the study area; x_i and x_j represent the observed values of a certain attribute on the x -space regional unit; \bar{x} is the mean of the research object x ; W_{ij} is the spatial weight matrix. If Moran's I is significantly positive, then the areas with higher (or lower) ecological vulnerability levels are spatially significantly clustered. Conversely, if Moran's I is significantly negative, then there is a significant spatial difference in the ecological vulnerability levels of the region and the surrounding area.

– Getis-Ord G_i^*

Getis-Ord G_i^* is used to identify the high-value and low-value agglomeration areas at different spatial positions, i.e., hot spots and cold spots [66].

$$EG_i^*(d) = \frac{\sum_{j=1}^n W_{ij}(d)X_j}{\sum_{j=1}^n X_j} \quad (14)$$

$$Z(G_i^*) = \frac{G_i^* - E(G_i^*)}{\sqrt{\text{Var}(G_i^*)}} \quad (15)$$

...where W_{ij} is the spatial weight matrix, the spatial adjacency is 1, and the non-adjacent is 0. $E(G_i^*)$ is the mathematical expectation, and $\text{Var}(G_i^*)$ is the compilation number of G_i^* . If $Z(G_i^*)$ is positive and significant, then the value around position i is relatively high (above the mean), which is the high-value spatial clustering (hot spot area); if $Z(G_i^*)$ is negative and significant, then the value around position i is relatively low (below average), which belongs to the low-value spatial clustering (cold spot area).

(2) Geographical detectors method

According to Wang (2017), a geographical detector is used to detect the spatial differences in

Table 1. Independent variables of ecological vulnerability.

Variables	Standard of Classification
Elevation (x_1)	Calculated from DEM data, the data is divided into 5 categories by natural fracture method
Slope (x_2)	Calculated from DEM data, the data is divided into 5 categories by natural fracture method
Precipitation (x_3)	Classed into five categories with natural breaks
Temperature (x_4)	Classed into five categories with natural breaks
Land use type (x_5)	Categorized into: bare-rock area, glaciers, water bodies, low coverage meadow, medium coverage meadow, high coverage meadow, forest, agricultural area and construction area
Distance from road (x_6)	Calculated the distance from road, the data is divided into 5 categories by natural fracture method
Distance from tourist attraction (x_7)	Calculated the distance from tourist attraction, the data is divided into 5 categories by natural fracture method
Distance from settlements (x_8)	Calculated the distance from settlements, the data is divided into 5 categories by natural fracture method

geographical elements. The geographical detector includes a differentiation factor detector, risk detector, interaction detector, and ecological detector [67]. Differentiation factor detector is used to analyze the interpretation degree of the influencing factor to the research object. Interaction detector can identify the explanatory power of two factors to the research object under the interaction. Geographical detectors are better at processing the algorithms for classified data than for continuous data. In this study, we selected the differentiation factor detector and the interaction detector to study the influencing factors and mechanisms of ecological vulnerability [68].

– Differentiation factor detector

This model detects the spatial differentiation of Y and probes how much factor x explains the spatial differentiation of Y.

$$q = 1 - \frac{1}{n\sigma^2} \sum_{h=1}^L N_h \sigma_h^2 \tag{16}$$

...where q is the indicator of the spatial differentiation detection of the dependent variable; $h = 1, \dots, L$ is the stratification of variables or factors; N_h is the number of sub-level regional sample units; N is the number of sample units in the entire region; L is the number of secondary regions; σ^2 is the variance of the dependent variable for the entire region; σ_h^2 is the variance of the second-level region. The value interval of q is [0, 1]. The larger the q value, the higher the degree of spatial differentiation of the dependent variable. If the stratification is generated by independent variables, the greater the value of q, the stronger the explanatory power of the independent variable. When $q = 0$, the independent variable has no relationship with the dependent variable. When $q = 1$, the independent variable completely controls the dependent variable.

– Interaction detector

The model can identify the interactions between different factors and assess whether the influencing

factors will increase or decrease the explanatory power of the dependent variable when they work together, or the influence of these factors on the dependent variable is independent. First, the factors (x_1 and x_2) are calculated for dependent variable q ($q(x_1)$ and $q(x_2)$). Then, the interactive variable q ($q(x_1 \cap x_2)$) is calculated under the interaction of several factors. Finally, $q(x_1)$, $q(x_2)$, and $q(x_1 \cap x_2)$ are compared. When $q(x_1 \cap x_2)$ is higher than the sum of x_1 and x_2 , then x_1 and x_2 have a non-linear strengthening effect. When $q(x_1 \cap x_2)$ is higher than the individual values of x_1 and x_2 , and $q(x_1 \cap x_2)$ is less than the sum of x_1 and x_2 , then x_1 and x_2 have a mutual strengthening effect [5].

Based on the existing research and data accessibility, the main influencing factors of elevation (x_1), slope (x_2), precipitation (x_3), temperature (x_4), land use type (x_5), distance from road (x_6), distance from tourist attractions (x_7), and distance from settlements (x_8) were used to explain the ecological vulnerability of the study area. According to the data requirements of the geographical detectors model, ecological vulnerability was used as the dependent variable, and the influencing factors were classified via the natural fracture method. In ArcGIS 10.5 software, vector points and fishnet vector data with the size of 30 m × 30 m were generated. The dependent and independent variables were matched through each vector point to detect the contribution of influencing factors (Table 1).

Results

Characteristics of Ecological Vulnerability Indicators

The values of NDVI, WET, NDISI, and LST showed differences in 2000 and 2017. From 2000 to 2017, the values of WET, NDISI, and LST in the TSA showed an upward trend, with their average values rising from -0.1076, 0.0042, and 9.5960 to -0.0616, 0.0241,

Table 2. The result of spatial component principle analysis.

PC	Eigenvalues		Contribution ratio of Eigenvalues/%		Cumulative contribution of Eigenvalues/%	
	2000	2017	2000	2017	2000	2017
1	0.0253	0.0146	62.4558	52.4522	62.4558	52.4522
2	0.0090	0.0087	22.2822	31.0644	84.7380	83.5116
3	0.0043	0.0036	10.5998	13.0116	95.3379	96.5279
4	0.0019	0.0010	4.6621	3.4721	100.0000	100.0000

Table 3. Statistics of NDVI, WET, NDISI, LST during 2000-2017.

	Statistics	Max	Min	Mean	Std
2000	NDVI	1	-1	0.3819	0.2588
	WET	0.5805	-0.4646	-0.1076	0.1473
	NDISI	0.4500	-0.6500	0.0042	0.2034
	LST	31.0513	-25.1337	9.5960	9.1505
2017	NDVI	1	-1	0.3579	0.2802
	WET	1.1135	-0.2784	-0.0616	0.1158
	NDISI	1	-1	0.0241	0.2302
	LST	43.1841	-17.8275	19.1933	10.0547

increased. The value of LST changed the most; the maximum and minimum values were different, and the mean value was higher than that of the other indicators. The value of WET changed the least, and the mean value was also lower than that of the other indicators. The average value of NDVI decreased slightly from 0.3819 to 0.3579. From 2000 to 2017, the standard deviation of NDVI, NDISI, and LST increased, indicating large differences in greenness, dryness, and heat (Table 3).

The spatial distribution of ecological vulnerability indicators shows that the area of the bare land in the study area increased; thus, the surface dryness and LST also increased, during 2000-2017. With the establishment of ecological conservation measures, such as the demolition of hotels, guesthouses, and infrastructure within the scenic area, vegetation coverage and soil moisture have improved, and the ecological factors have developed in the favorable direction in the residential area in the north of TSA (Fig. 3).

and 19.1933, with an increase of 42.75% 473.81%, and 100.01%, which indicates that the water conservation capacity of the research area improved, and surface temperature and the degree of surface exposure

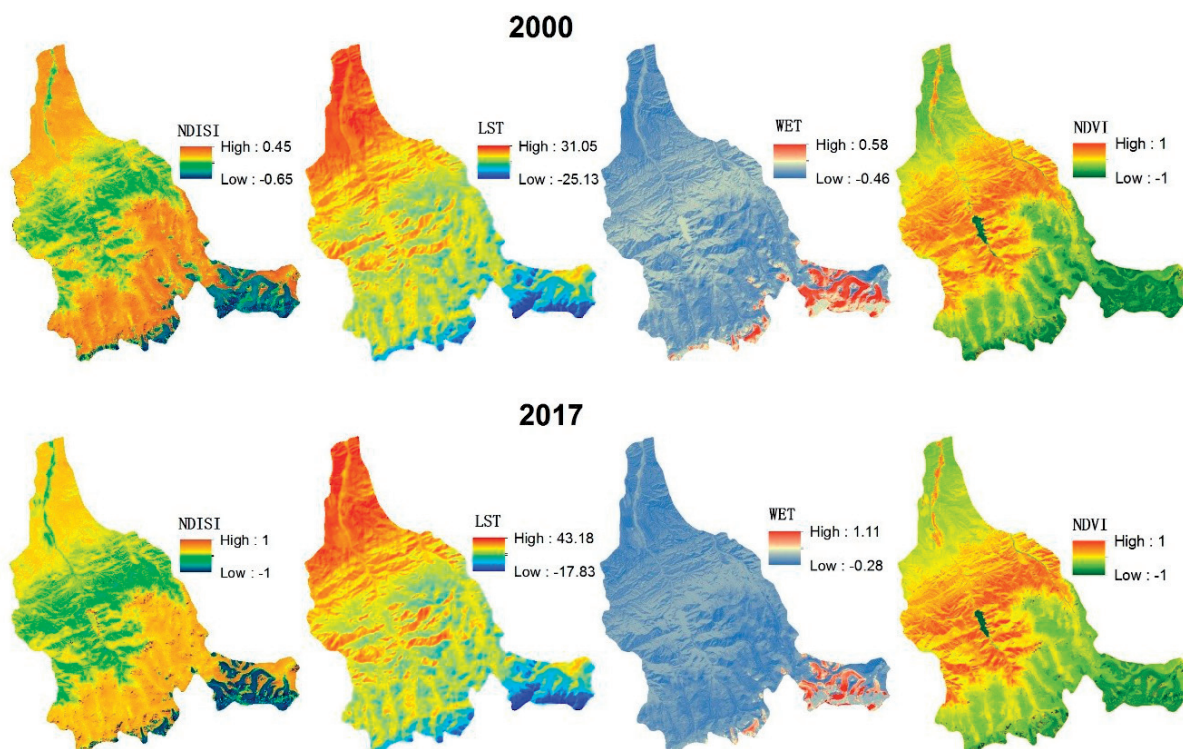


Fig. 3. Characteristics of ecological vulnerability indicators in TSA.

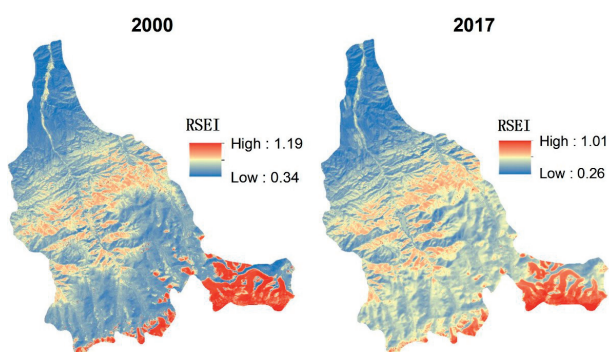


Fig. 4. Spatial distribution of RSEI in TSA.

Temporal and Spatial Evolution Pattern of Ecological Vulnerability

According to the PCA, the evaluation model of the RSEI in 2007 and 2017 can be expressed as follows.

$$RSEI_{2007} = 0.6246PC_1 + 0.2228PC_2 + 0.1060PC_3$$

$$RSEI_{2017} = 0.5245PC_1 + 0.3106PC_2 + 0.1301PC_3$$

$RSEI_{2007}$ and $RSEI_{2017}$ are the remote sensing ecological indices of 2007 and 2017, respectively, and PC_1-PC_3 are the first three principal components after the principal component transformation of the original spatial variables.

In 2007 and 2017, the cumulative contribution rate of the three principal components reached 95%, which is greater than 85%; thus, the fourth principal component in these two years can be ignored (Table 2).

The RSEI was used to represent the spatial distribution of ecological vulnerability levels in 2000 and 2017. The RSEI showed a downward trend from 2000 to 2017. The highest value decreased by 23.53% from 1.19 to 1.01, and the minimum value decreased by 15.12% from 0.34 to 0.26 (Fig. 4).

In 2000 and 2017, the regions of grades I, II, and III in the study area were dominant, and the overall ecological vulnerability was low. The areas of grades I, II, and V decreased by 33.56 km², 32.80 km², and 8.94 km², respectively, and those of grades III

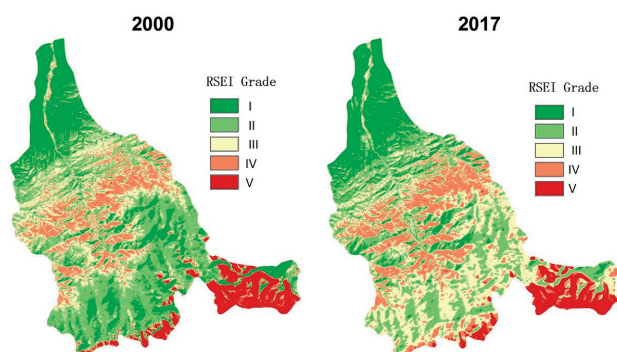


Fig. 5. Regions of grades to RSEI in TSA.

and IV increased slightly by 50.60 km² and 24.69 km² (Fig. 5).

In 2000, the areas of the RSEI grades I–V were 128.11 km², 188.59 km², 111.40 km², 67.38 km², and 43.02 km², respectively. The areas of grades I, II, and III (low ecological vulnerability) accounted for 79.5%, while those of grades IV and V (high ecological vulnerability) were smaller, 110.40 km². The region of grade I is distributed in the temperate desert belt, mountain steppe belt, and partly in the alpine cushion vegetation belt in the north of TSA. The land use type of this region is low- and medium-coverage grassland and part bare land. The area of grade II region is the largest, and it is mostly in the alpine cushion vegetation belt and partly in the mountain coniferous forest belt, which is dominated by bare land and partly by the high-coverage grassland. The grade III region is mostly in the mountain coniferous forest belt, subalpine-alpine meadow belt, and partly in the northern residential agglomeration area along the Sangong River valley. The grade IV region is dominated by the mountainous coniferous forest belt. The grade V area has the smallest area and is distributed in the glacial snow belt in the northern part of the study area.

In 2017, the areas of RSEI grades I–V were 94.64 km², 156.03 km², 162.42 km², 92.32 km², and 34.84 km², respectively. The areas of grades I, II, and III (low ecological vulnerability) accounted for 76.46%, while the areas of grades IV and V (high ecological vulnerability) were 127.16 km². The area of grade I, which extends to the southern part of the mountain steppe belt, decreased while the region in the alpine cushion vegetation belt disappeared. The area of grade II region decreased. However, in the alpine cushion vegetation belt, the distribution changed from the flake to the point, and the region became more fragmented. The area of grade III and IV increased. The grade IV region extends to the snow belt in the south. The area of the grade V region, which is still mainly distributed in the glacial snow belt, decreased (Fig. 6).

Spatial Heterogeneity of RSEI

Using Geoda software, the Moran's I value of the RSEI was calculated. The spatial correlation of

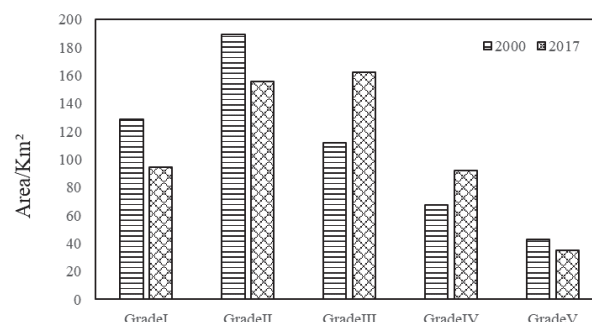


Fig. 6. Area of ecological vulnerability grades.

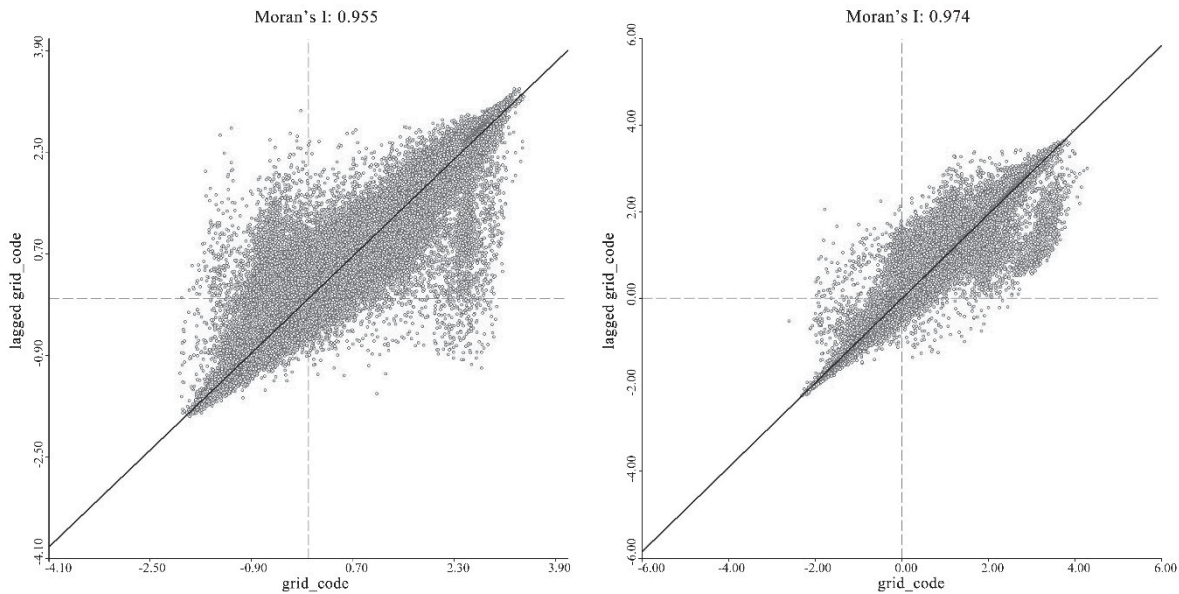


Fig. 7. Moran scatterplot of RSEI during 2000-2017.

the RSEI combining the scatter plot and the hot-cold spot spatial distribution map was analyzed. Moran's I in 2000 and 2017 passed the significance test ($p = 0.01 < 0.05$). Moran's I was greater than 0.5, implying that the ecological environment in the TSA had a positive autocorrelation or a highly clustered pattern. From 2000 to 2017, the value of Moran's I increased from 0.955 to 0.974, indicating that the ecological vulnerability of the study area was stable during the 17-year period. The spatial positive correlation of ecological vulnerability in the study area showed strong spatial agglomeration (Fig. 7).

To study the pattern evolution of ecological vulnerability, we used Getis-Ord G^* to calculate the spatial correlation in the distribution of the RSEI and identify the hot spots (high-high) and cold spots (low-low). From 2000 to 2017, the RSEI showed positive

spatial agglomeration in hot and cold spots, and the distribution pattern showed significant differences. The cold-hot spots in the study area showed the characteristics of "cold spots-hot spots-cold spots-hot spots" alternating from north to south. The distribution of cold and hot spots shows obvious vertical zonality.

In 2000, the cold spot areas were mainly distributed in the temperate desert belt and alpine cushion vegetation belt, partly scattered in the mountain steppe belt and mountain coniferous forest belt. In 2017, the cold spot areas in the north extended to the south, gradually transitioning from the temperate desert belt to the mountain steppe belt. The cold spot areas in the mountain coniferous forest belt also increased; whereas, those in the southern alpine cushion vegetation belt decreased, and the distribution changed from the banded cluster to the dotted random distribution.

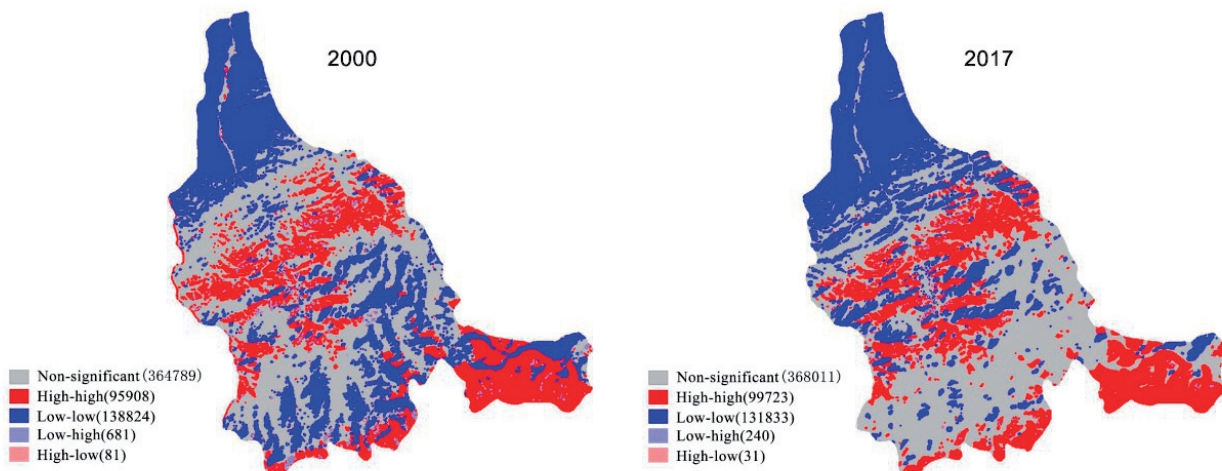


Fig. 8. The distribution of spatial associations type in TSA.

Table 4. The contribution value of factors to RSEI in 2000 and 2017.

Factors	q ₂₀₀₀ Statistic	q ₂₀₁₇ Statistic	Absolute change of q Statistic	Relative change of q Statistic
Elevation (x ₁)	0.3140***	0.3839***	0.0699	22.27%
Slope (x ₂)	0.0223***	0.0685***	0.0462	207.44%
Precipitation (x ₃)	0.3029***	0.3852***	0.0823	27.16%
Temperature (x ₄)	0.3003***	0.3918***	0.0915	30.48%
Land Use Type (x ₅)	0.6803***	0.6652***	-0.0151	-2.22%
Distance from road (x ₆)	0.0432***	0.0293***	-0.0139	-32.20%
Distance from tourist attraction (x ₇)	0.2024***	0.2458***	0.0434	21.46%
Distance from settlements (x ₈)	0.1740***	0.2215***	0.0474	27.26%

In 2000, hot spot areas were mainly distributed in mountainous coniferous forest belts and glacial snow belts, and scattered in the Sangong River basin. In 2017, the hot spot areas in the mountain coniferous forest belt gathered slightly to the south and extended south to the alpine cushion vegetation belt. The hot spot areas in the snow belts did not change significantly, and the sporadic hot spot areas in the Sangong River transformed into insignificant areas (Fig. 8).

Detected Factors of Ecological Vulnerability

Based on the results of the geographical detectors model, the influencing factors of the RSEI passed the significance test ($p < 0.001$). In 2000, the q values of the factors were as follows: land type (0.6803) > elevation (0.3140) > precipitation (0.3029) > temperature (0.3003) > tourism (0.2024) > community resident (0.1740) > road (0.0432) > slope (0.0223). The q values of the factors in 2017 were as follows: land type (0.6652) > temperature (0.3918) > precipitation (0.3852) > elevation (0.3839) > tourism (0.2458) > community resident (0.2215) > slope (0.0685) > road (0.0293). In 2000 and 2017, the factor of land use type (x₅) had the largest contribution, with a contribution value greater than 0.5, followed by the value of elevation (x₁), temperature (x₄), and precipitation (x₃). The slope (x₂) factor had the lowest contribution value. In 2017, the contribution value of factors to the RSEI increased, the values of elevation (x₁), slope (x₂), precipitation (x₃), temperature (x₄), tourism (x₇), and community resident (x₈) increased by 22.27%, 207.44%, 27.16%, 30.48%, 21.46%, and 27.26%, respectively (Table 4).

The results of the geographical detectors model show that the impact of the interactions of any two factors on the RSEI is greater than the impact of a single variable. The explanatory value of any two mutually reinforcing factors was calculated. Overall, the explanatory value of land use type (x₅) is the highest; thus, the explanatory power of the combination of land use type (x₅) and other factors is significantly higher

than that of the other factors. In 2000, the combination of land use type (x₅) and precipitation (x₃) factors had the largest explanatory value of 0.7053, followed by the factors of elevation and land use type (x₁ ∩ x₅), with an explanatory power of 0.7046. In 2017, the explanatory power of various factors increased, but there was also a decline in the explanatory power among the factors because of the decline in the explanatory power of the single factor of the land use type (x₅). The combination of land use type (x₅) and temperature (x₄) factors had the largest explanatory value of 0.7064, followed by the factors of precipitation and land use type (x₃ ∩ x₅), with an explanatory power of 0.7061. In 2017, the explanatory power between elevation (x₁) and slope (x₂) changed from nonlinear strengthening to mutual strengthening effect, and the explanatory power between the distance from road (x₆) and the distance from tourist attractions (x₇) changed from mutual strengthening to nonlinear strengthening (Table 5).

Discussion

Spatial and Temporal Evolution of Ecological Vulnerability

The ecological vulnerability zoning in this study is based on the RSEI, which represents the combined effect of greenness, wetness, dryness, and heat. From 2000 to 2017, the values of greenness, wetness, dryness, and heat changed in space, which were represented by the indicators of NDVI, WET, NDISI, and LST. According to the result of the PCA, the indicator of LST is ignored. Therefore, the value of RSEI was calculated by NDVI, WET, NDISI. NDISI is positive indicators, and NDVI and WET are reverse indicators to RSEI. The value of NDVI decreased. And the results of PCA showed that the contribution value of NDVI to RSEI decreased. The value of WET increased and the contribution value to RSEI increased. Although the value of NDISI increased, the value changed little and

Table 5. Interaction between different factors to RSEI in 2000 and 2017.

$L = x_i \cap x_j$	$q_{2000}(x_i \cap x_j)$	Result ₂₀₀₀	Explanatory	$q_{2017}(x_i \cap x_j)$	Result ₂₀₁₇	Explanatory
$x_1 \cap x_2$	0.3376	$L > x_1 + x_2$	$x_1 \nearrow x_2$	0.4002	$L > x_1, x_2; L < x_1 + x_2$	$x_1 \uparrow \uparrow x_2$
$x_1 \cap x_3$	0.3802	$L > x_1, x_3; L < x_1 + x_3$	$x_1 \uparrow \uparrow x_3$	0.4245	$L > x_1, x_3; L < x_1 + x_3$	$x_1 \uparrow \uparrow x_3$
$x_1 \cap x_4$	0.3887	$L > x_1, x_4; L < x_1 + x_4$	$x_1 \uparrow \uparrow x_4$	0.4384	$L > x_1, x_4; L < x_1 + x_4$	$x_1 \uparrow \uparrow x_4$
$x_1 \cap x_5$	0.7046	$L > x_1, x_5; L < x_1 + x_5$	$x_1 \uparrow \uparrow x_5$	0.7037	$L > x_1, x_5; L < x_1 + x_5$	$x_1 \uparrow \uparrow x_5$
$x_1 \cap x_6$	0.3634	$L > x_1 + x_6$	$x_1 \nearrow x_6$	0.4192	$L > x_1 + x_6$	$x_1 \nearrow x_6$
$x_1 \cap x_7$	0.3862	$L > x_1, x_7; L < x_1 + x_7$	$x_1 \uparrow \uparrow x_7$	0.4436	$L > x_1, x_7; L < x_1 + x_7$	$x_1 \uparrow \uparrow x_7$
$x_1 \cap x_8$	0.3947	$L > x_1, x_8; L < x_1 + x_8$	$x_1 \uparrow \uparrow x_8$	0.4280	$L > x_1, x_8; L < x_1 + x_8$	$x_1 \uparrow \uparrow x_8$
$x_2 \cap x_3$	0.3227	$L > x_2, x_3; L < x_2 + x_3$	$x_2 \uparrow \uparrow x_3$	0.4031	$L > x_2, x_3; L < x_2 + x_3$	$x_2 \uparrow \uparrow x_3$
$x_2 \cap x_4$	0.3132	$L > x_2, x_4; L < x_2 + x_4$	$x_2 \uparrow \uparrow x_4$	0.4033	$L > x_2, x_4; L < x_2 + x_4$	$x_2 \uparrow \uparrow x_4$
$x_2 \cap x_5$	0.6854	$L > x_2, x_5; L < x_2 + x_5$	$x_2 \uparrow \uparrow x_5$	0.6768	$L > x_2, x_5; L < x_2 + x_5$	$x_2 \uparrow \uparrow x_5$
$x_2 \cap x_6$	0.0823	$L > x_2 + x_6$	$x_2 \nearrow x_6$	0.1138	$L > x_2 + x_6$	$x_2 \nearrow x_6$
$x_2 \cap x_7$	0.2150	$L > x_2, x_7; L < x_2 + x_7$	$x_2 \uparrow \uparrow x_7$	0.2705	$L > x_2, x_7; L < x_2 + x_7$	$x_2 \uparrow \uparrow x_7$
$x_2 \cap x_8$	0.2257	$L > x_2 + x_8$	$x_2 \nearrow x_8$	0.2962	$L > x_2 + x_8$	$x_2 \nearrow x_8$
$x_3 \cap x_4$	0.3658	$L > x_3, x_4; L < x_3 + x_4$	$x_3 \uparrow \uparrow x_4$	0.4292	$L > x_3, x_4; L < x_3 + x_4$	$x_3 \uparrow \uparrow x_4$
$x_3 \cap x_5$	0.7053	$L > x_3, x_5; L < x_3 + x_5$	$x_3 \uparrow \uparrow x_5$	0.7061	$L > x_3, x_5; L < x_3 + x_5$	$x_3 \uparrow \uparrow x_5$
$x_3 \cap x_6$	0.3926	$L > x_3 + x_6$	$x_3 \nearrow x_6$	0.4434	$L > x_3 + x_6$	$x_3 \nearrow x_6$
$x_3 \cap x_7$	0.3752	$L > x_3, x_7; L < x_3 + x_7$	$x_3 \uparrow \uparrow x_7$	0.4439	$L > x_3, x_7; L < x_3 + x_7$	$x_3 \uparrow \uparrow x_7$
$x_3 \cap x_8$	0.4090	$L > x_3, x_8; L < x_3 + x_8$	$x_3 \uparrow \uparrow x_8$	0.4477	$L > x_3, x_8; L < x_3 + x_8$	$x_3 \uparrow \uparrow x_8$
$x_4 \cap x_5$	0.7011	$L > x_4, x_5; L < x_4 + x_5$	$x_4 \uparrow \uparrow x_5$	0.7064	$L > x_4, x_5; L < x_4 + x_5$	$x_4 \uparrow \uparrow x_5$
$x_4 \cap x_6$	0.3753	$L > x_4 + x_6$	$x_4 \nearrow x_6$	0.4393	$L > x_4 + x_6$	$x_4 \nearrow x_6$
$x_4 \cap x_7$	0.3762	$L > x_4, x_7; L < x_4 + x_7$	$x_4 \uparrow \uparrow x_7$	0.4483	$L > x_4, x_7; L < x_4 + x_7$	$x_4 \uparrow \uparrow x_7$
$x_4 \cap x_8$	0.3917	$L > x_4, x_8; L < x_4 + x_8$	$x_4 \uparrow \uparrow x_8$	0.4419	$L > x_4, x_8; L < x_4 + x_8$	$x_4 \uparrow \uparrow x_8$
$x_5 \cap x_6$	0.6883	$L > x_5, x_6; L < x_5 + x_6$	$x_5 \uparrow \uparrow x_6$	0.6699	$L > x_5, x_6; L < x_5 + x_6$	$x_5 \uparrow \uparrow x_6$
$x_5 \cap x_7$	0.7046	$L > x_5, x_7; L < x_5 + x_7$	$x_5 \uparrow \uparrow x_7$	0.6959	$L > x_5, x_7; L < x_5 + x_7$	$x_5 \uparrow \uparrow x_7$
$x_5 \cap x_8$	0.6906	$L > x_5, x_8; L < x_5 + x_8$	$x_5 \uparrow \uparrow x_8$	0.6767	$L > x_5, x_8; L < x_5 + x_8$	$x_5 \uparrow \uparrow x_8$
$x_6 \cap x_7$	0.2546	$L > x_6, x_7; L < x_6 + x_7$	$x_6 \uparrow \uparrow x_7$	0.2834	$L > x_6 + x_7$	$x_6 \nearrow x_7$
$x_6 \cap x_8$	0.2009	$L > x_6, x_8; L < x_6 + x_8$	$x_6 \uparrow \uparrow x_8$	0.2419	$L > x_6, x_8; L < x_6 + x_8$	$x_6 \uparrow \uparrow x_8$
$x_7 \cap x_8$	0.3463	$L > x_7, x_8; L < x_7 + x_8$	$x_7 \uparrow \uparrow x_8$	0.4196	$L > x_7, x_8; L < x_7 + x_8$	$x_7 \uparrow \uparrow x_8$

its contribution value to RSEI was significantly less than that of NDVI and WET. In the superposition of three values, the value of RSEI decreased from 2000 to 2017. As a result, a reduction in the NDVI value did not increase the RSEI, which had no impact on RSEI.

Ecological vulnerability zones of the same grade showed spatial differences, and hot and cold spots in the study area alternated. Different grades of ecological vulnerability have different influencing factors. The distribution of the region of grade I is consistent with the cold spot area of the RSEI. It is mainly distributed in the temperate desert belt, mountain steppe belt, and some alpine cushion vegetation belt to the north of the study area, with low- and medium-coverage grassland

and some bare land. According to the field survey conducted in 2018-2019, the main plant types in the area are temperate semi-shrubs and dwarf semi-shrubs, such as *Caragana soongorica*, *Seriphidium borotalense*, and *Ceratoides latens*. The species diversity and richness are low in this area. The values of Simpson, Shannon-Wiener, and Margalef indices were less than 0.5 (Table 6). The result of this partition is consistent with the findings of Shi (2019), which showed that the basic characteristics of the ecological environment in this area are poor [19, 69]. When the area is subjected to external forces or human interference, its ecological environment did not change significantly. The local government implemented strict protection

Table 6. Species diversity of under different ecological vulnerability grades in 2018-2019.

Species diversity	Grade I	Grade II	Grade III	Grade IV	Grade V
Simpson index	0.4527	0.5100	0.6720	0.6179	0.1352
Shannon-Wiener diversity index	0.3054	0.3844	0.5043	0.4933	0.1285
Margalef richness indexes	0.2097	0.2611	0.3613	0.4568	0.4997
Number of dominant species	0.1750	0.1806	0.2028	0.2625	0.3542
Average height of dominant species	0.0300	0.3037	0.2167	0.1950	0.3972
Total coverage	0.4667	0.8210	0.8662	0.8811	0.8130

and management measures for the TSA in 2012, such as banning the mining activities and the relocation of herdsmen, which decreased the ecological vulnerability [40].

The distribution of the region of grade II changed from 2000 to 2017. This area is mainly distributed in alpine cushion vegetation belts and some mountainous coniferous forest belts. The alpine cushion vegetation belt is dominated by the dominant species of *Trollius lilacinus* Bunge, *Rhodiola rosea* L., *Saxifraga stolonifera* Curt., and *Saussurea involucrata* (Kar. et Kir.) Sch.-Bip [70, 71]. The species diversity, richness, and vegetation coverage of the grade II area are slightly higher than those of the grade I area but still poor mostly because of the human activity and grazing. Since 2012, the local government has implemented policies of banning, restricting, and rotating grazing, as well as strict supervision and protection measures in the area. The size of the area decreased in 2017, which shows that the vulnerability of the ecological environment decreased and the implementation of the policies improved the ecological environment [19, 72].

The region of grade III is concentrated in the mountainous coniferous forest belt, subalpine-alpine meadow belt, and partly in the residential area along the Sangong River basin in the north. The vegetation in the area is mainly temperate grass, weedy meadows, and alpine artemisia, such as *Alchemilla japonica*, *Geranium wilfordii* Maxim., and *Polygonum viviparum* L. The species diversity, richness, and vegetation coverage in this area are high [44, 48]. The values of Simpson and Shannon-Wiener indices are greater than 0.5. Since 2013, the government has implemented a strict management system for tourism activities and demolished some infrastructure in the tourist areas. Therefore, although the area of this grade increased in the past 17 years, the overall ecological environment vulnerability improved after the implementation of the policies [73].

The region of grade IV is distributed in the mountainous coniferous forest belts, which is consistent with the distribution of some hot spots in the RSEI. This region has *Betula tianschanica* Rupr, *Larix sibirica* Ledeb, *Sabina pseudosabina* and *Picea schrenkiana*. The area has abundant precipitation, high

species diversity, and richness (the values of Simpson and Shannon-Wiener indices are greater than 0.5), and good vegetation coverage (the value of total coverage was greater than 0.5). This area has the richest species diversity in the TSA [40]. *Picea schrenkiana* in this area is a typical vegetation group in the Xinjiang Tianshan heritage site and has a unique bio-ecological value in the arid region. When the region was subjected to external forces or human interference, the ecological environment changed [74]. The Tianchi Lake in this area is an important viewing point and gathering place for tourists. Tourists have a significant impact on the surrounding ecological environment [37, 75]. From 2000 to 2017, the size of the area increased, its range extended to the snow belt, and the distribution was fragmented in the north. Since the local government in the TSA has implemented policies to protect the landscape and supervise the tourist activities in 2012, the region was less affected by human activities [38, 76]. Therefore, the changes in the region can be attributed to the variations in temperature, precipitation, and government policies [77].

The region of grade V is distributed in the snow belt, which coincides with the hot spots of the RSEI. The Quaternary glacial erosion and moraine landform types, such as the ancient glacial landscape of tind, aretes, U-shaped valleys, cirques, sheep back stones, boulders, glaciarium, and moraine-dammed lakes, are completely preserved in this region [78, 79]. Due to its high altitude and poor vegetation distribution, the region lacks the ability of self-renewal and recovery. The reason this area becomes smaller is the climate change, which considerably decreases the glacier area [45, 79].

Factors of Ecological Vulnerability

The assessment of the factors of the temporal and spatial changes in ecological vulnerability showed that the land use type is the main factor, followed by temperature, precipitation, and elevation.

The land use type is the surface complex covered by the earth's natural surface covering and various artificial buildings. It is determined by human activities such as crop selection, crop layout, input, and power.

Its changes reflect the state of the ecological environment, and the degree of interference of human activities on nature [80]. Ecological vulnerability is determined by the natural conditions, and is also affected by human activities. Wang (2008) believed that different land use types resulted in different degree of ecological vulnerability. The land use types that are suitable for the ecological environment are conducive to the improvement and stability of the land ecological environment, enabling the healthy development and reduce ecological vulnerability. Improper man-made utilization will cause the patch fragmentation of land use types [80]. This fragmented feature increases the degree of isolation between habitat patches, resulting in reduced biodiversity, destruction of ecosystems, and deterioration of the original environmental quality [81,82]. In this paper, land use type has the highest impact on ecological vulnerability, which reflects the greenness, wetness, dryness, and heat of the region. The results of this paper are consistent with those of the above scholars, and verify the effect of land use types on ecological vulnerability.

Climate change causes the changes in regional distribution of water and heat, affecting the distribution of vertical natural belts, the structure of ecological communities, and the biodiversity of habitats [83]. Temperature and precipitation directly affect vegetation coverage, soil moisture, and surface temperature. From 1989 to 2016, the distribution of vertical natural belts in the study area changed significantly due to the combined influence of temperature and precipitation. Among them, the lower limit of the forest belt decreased by 25 m, the upper line rose by 24 m, so the mountain coniferous forest belt expanded, and the suitable growth range of *Picea schrenkiana* became wider [44]. Temperature and precipitation also play a very important role in the pattern and development of grassland, and the influence of temperature on the grassland ecosystem is lower than that of precipitation. Temperature and precipitation will inevitably affect the distribution of grassland, causing vegetation to migrate within a certain range [83]. In addition, climate change may also lead to the disappearance or extinction of species in some areas. In some hot spots, climate change may cause 43% of species to disappear, that is, about 56,000 local plants and 3700 local vertebrates will be extinct [84]. The research in this paper is consistent with the above scholars, which verifies the importance of temperature and precipitation to ecological vulnerability and have a significant impact on regional ecosystems.

Topographic factors determine the climate, land use type and the distribution of vertical belt in the study area, which are important factors affecting the spatial pattern of land use, vegetation and soil distribution [85]. The change in terrain directly affects the flow of material on the ground and the conversion of energy, which has obvious restrictions on human production and life, and makes the distribution of land use types on the terrain gradient show regular changes [86].

Elevation is an important digital parameter of terrain factor. With the change of elevation, temperature and precipitation change significantly, which have effects on land use types, vegetation coverage, and soil moisture. Obviously, it leads to obvious changes in ecological vulnerability. The results of this study are consistent with the above studies, reflecting the significant effect of elevation factors on the regional ecological vulnerability [86-88].

Limitations and Future Trends

The purpose of selecting the RSEI in this study was to objectively reflect the vulnerability of the ecological environment in the TSA, and to make a real and objective assessment of the regional ecological environment [53]. The RSEI ecological indicator is not subject to human factors and subjective conditions [30]. It can not only achieve the objective quantitative assessment of the ecological status of the region, but also reveal the spatial and temporal analysis of the evolution of the ecological environment [89, 90]. The RSEI can objectively reflect the vegetation coverage, soil conditions, surface bareness, and surface temperature in the area [29, 35]. The comprehensive index weighted by greenness, wetness, dryness, and heat can not only overcome the disadvantages of using a single index, but also makes the integration of each subindex more reasonable. In addition, the index weights were objectively determined using PCA, which can reduce the uncertainty caused by human factors and avoid the ecological vulnerability caused by the subjective weight setting [2, 33, 62, 91, 92].

One of the limitations of this study is that we only used the remote sensing image data for two years, and the analysis of the evolution of the ecological environment was not clear. Second, the study area has obvious vertical natural belt characteristics, and the vegetation types, diversity, coverage, and soil types of the different vertical natural belts in the study area showed significant differences [3]. This study has not explored the reasons of the ecological vulnerability of the study area from 2000 to 2017 from the perspective of vertical natural belts. In future research, the reasons for the changes in ecological vulnerability will be explored from the perspective of the vertical natural belts of the mountains to scientifically reflect the spatial and temporal characteristics of the ecological vulnerability of the mountain natural heritage sites and to achieve sustainable development [34, 54].

Conclusions

In this study, RSEI was used to analyze the ecological vulnerability in the TSA. With the spatial statistical model and geographical detectors model, the spatial distribution characteristics of the study area in 2000 and 2017, and the influencing factors were

detected. The results showed that: (1) From 2000 to 2017, the values of greenness, wetness, dryness, and heat changed in space. The values of WET, NDISI, and LST increased, and the value of NDVI decreased. The spatial distribution of indicators to RSEI shows that the area of the bare land in the study area increased. But, with the establishment of ecological conservation measures, the ecological factors have developed in the favorable direction in the residential area in the north of TSA. (2) According to the result of the PCA, the value of RSEI was calculated by NDVI, WET and NDISI. In the superposition of three values, the value of RSEI decreased from 2000 to 2017. Based on the RSEI value, grades I–V was used to determine the classification of ecological vulnerability from low to high. In 2000 and 2017, the regions of grades I, II, and III were dominant, and the overall ecological vulnerability was low. The area of grades I, II, and V decreased, grades III and IV increased. (3) From 2000 to 2017, the value of Moran's I increased, indicating that the ecological vulnerability of the study area was stable during the 17-year period, and the spatial positive correlation of ecological vulnerability showed strong spatial agglomeration. The cold-hot spots in the study area showed the characteristics of “cold spots-hot spots-cold spots-hot spots” alternating from north to south, and the distribution of cold and hot spots shows obvious vertical zonality. (4) The results of the geographical detectors model showed that the factor of land use type (x_5) had the largest contribution, followed by the value of elevation (x_1), temperature (x_4), and precipitation (x_3). The slope (x_2) factor had the lowest contribution value. The impact of the interactions of any two factors on the RSEI is greater than the impact of a single variable. The explanatory power of the combination of land use type (x_5) and other factors is significantly higher than that of the other factors. (5) The limitations of this study is that we only used the remote sensing image data for two years, and the analysis of the evolution of the ecological environment was not clear. In future research, the reasons for the changes in ecological vulnerability will be explored from the perspective of the vertical natural belts of the mountains to scientifically reflect the spatial and temporal characteristics of the ecological vulnerability of the mountain natural heritage sites and to achieve sustainable development.

Acknowledgements

This work was supported by the Provincial Natural Science Foundation of Xinjiang Uygur autonomous region (No. 2019D01A96), National Natural Science Foundation of China (No. 41661039).

Conflict of Interest

The authors declare no conflict of interest.

References

- LIU Y., ZHANG Z., TONG L., KHALIFA M., WANG Q., GANG C., WANG Z., LI J., SUN Z. Assessing the effects of climate variation and human activities on grassland degradation and restoration across the globe. *Ecological Indicators*, 106, **2019**.
- ZHANG X., YU W., CAI H., GUO X. Review of the evaluation methods of regional eco-environmental vulnerability. *Acta Ecologica Sinica*, **38** (16), 5970, **2018**.
- COOPS N.C., BOLTON D.K., HOBI M.L., RADELOFF V.C. Untangling multiple species richness hypothesis globally using remote sensing habitat indices. *Ecological Indicators*, 107, **2019**.
- SHAVYKIN A., KARNATOV A. Mapping of Ecological Vulnerability of Sea-Coastal Zones to Oil Spills: A Preliminary Method Applied to Kola Bay, the Barents Sea. *Journal of Marine Science and Engineering*, **7** (7), 216, **2019**.
- ZHU Q., ZHOU W.M., JIA X., ZHOU L., YU D.P., DAI L.M. Ecological vulnerability assessment on Changbai Mountain National Nature Reserve and its surrounding areas, Northeast China. *Ying yong sheng tai xue bao*, **30** (5), 1633, **2019**.
- TAI X., XIAO W., TANG Y. A quantitative assessment of vulnerability using social-economic-natural compound ecosystem framework in coal mining cities. *Journal of Cleaner Production*, 258, **2020**.
- TURNER B.L., KASPERSON R.E., MATSON P.A., MCCARTHY J.J., CORELL R.W., CHRISTENSEN L., ECKLEY N., KASPERSON J.X., LUERS A., MARTELLO M.L., POLSKY C., PULSIPHER A., SCHILLER A. A framework for vulnerability analysis in sustainability science. *Proceedings of the National Academy of Sciences of the United States of America*, **100** (14), 8074, **2003**.
- CUTTER S.L. The vulnerability of science and the science of vulnerability. *Annals of the Association of American Geographers*, **93** (1), 1, **2003**.
- PAAVOLA J. Livelihoods, vulnerability and adaptation to climate change in Morogoro, Tanzania. *Environmental Science & Policy*, **11** (7), 642, **2008**.
- ADGER W.N., Vulnerability. *Global Environmental Change-Human and Policy Dimensions*, **16** (3), 268, **2006**.
- DE L.H.J., SALA S., VIGHI M., FABER J.H. Ecological vulnerability in risk assessment - A review and perspectives. *Science of the Total Environment*, **408** (18), 3871, **2010**.
- ARETANO R., SEMERARO T., PETROSILLO I., DE M.A., PASIMENI M.R., ZURLINI G. Mapping ecological vulnerability to fire for effective conservation management of natural protected areas. *Ecological Modelling*, **295**, 163, **2015**.
- FUESSEL H.M. Vulnerability: A generally applicable conceptual framework for climate change research. *Global Environmental Change-Human and Policy Dimensions*, **17** (2), 155, **2007**.
- FRAZIER T.G., THOMPSON C.M., DEZZANI R.J. A framework for the development of the SERV model: A Spatially Explicit Resilience-Vulnerability model. *Applied Geography*, **51**, 158, **2014**.
- MA Z., MA S., ZHANG S. Ecological Vulnerability Assessment and Its Uncertainty Analysis of Dalian City. *Bulletin of Soil and Water Conservation*, **39** (3), 237, **2019**.

16. WEI X., ZHAO J., WEI W., XIE B. Spatial and temporal changes of ecological vulnerability per county unit in China. *Acta Scientiae Circumstantiae*, **36** (2), 726, **2016**.
17. GUPTA A.K., NEGI M., NANDY S., ALATALO J.M., SINGH V., PANDEY R. Assessing the vulnerability of socio-environmental systems to climate change along an altitude gradient in the Indian Himalayas. *Ecological Indicators*, 106, **2019**.
18. CHAUHAN N., SHUKLA R., JOSHI P.K. Assessing impact of varied social and ecological conditions on inherent vulnerability of Himalayan agriculture communities. *Human and Ecological Risk Assessment*, (11), 1, **2019**.
19. SHI H., SHI T., HAN F., LIU Q., WANG Z., ZHAO H. Conservation Value of World Natural Heritage Sites' Outstanding Universal Value via Multiple Techniques-Bogda, Xinjiang Tianshan. *Sustainability*, **11** (21), 1, **2019**.
20. ENEA M., SALEMI G. Fuzzy approach to the environmental impact evaluation. *Ecological Modelling*, **136** (2-3), 131, **2001**.
21. MA J., LI C., WEI H., MA P., YANG Y., REN Q., ZHANG, W. Dynamic evaluation of ecological vulnerability in the Three Gorges Reservoir Region in Chongqing Municipality, China. *Acta Ecologica Sinica*, **35** (21), 7117, **2015**.
22. LI S., WU S., DAI E. Assessing the fragility of ecosystem using artificial neural network model. *Acta Ecologica Sinica*, **25** (3), 621, **2005**.
23. TREVISAN D.P., BISPO P.D.C., ALMEIDA D., IMANI M., BALZTER H., MOSCHINI L.E. Environmental vulnerability index: An evaluation of the water and the vegetation quality in a Brazilian Savanna and Seasonal Forest biome. *Ecological Indicators*, 112, **2020**.
24. ZHOU X., GUO H., ZIBIBULA S., DENG Z., LIANG B. Change of remote sensing ecological index of an oasis city in the arid area. *Resources Science*, **41** (5), 1002, **2019**.
25. ZHANG N., CHEN D., XING F., LIU S., LI X., LI H. Ecological Change Analysis of Bole City in Arid Regions of Xinjiang Wei Autonomous Region Based on Remote Sensing Ecological Index. *Bulletin of Soil and Water Conservation*, **39** (1), 154, **2019**.
26. YAN M., WANG Y. Advances in the evaluation of ecological environmental quality. *Ecology and Environmental Sciences*, **21** (10), 1781, **2012**.
27. BADRELDIN N., GOOSSENS R. A satellite-based disturbance index algorithm for monitoring mitigation strategies effects on desertification change in an arid environment. *Mitigation and Adaptation Strategies for Global Change*, **20** (2), 263, **2015**.
28. LV X., XIAO W., ZHAO Y., ZHANG W., LI S., SUN H. Drivers of spatio-temporal ecological vulnerability in an arid, coal mining region in Western China. *Ecological Indicators*, 106, **2019**.
29. WANG L., JIAO L., LAI F., ZHANG N. Evaluation of ecological changes based on a remote sensing ecological index in a Manas Lake wetland, Xinjiang. *Acta Ecologica Sinica*, **39** (8), 2963, **2019**.
30. YANG J.Y., WU T., PAN X.Y., DU H.T., LI J.L., ZHANG L., MEN M.X., CHEN Y. Ecological quality assessment of Xiongan New Area based on remote sensing ecological index. *Ying yong sheng tai xue bao*, **30** (1), 277, **2019**.
31. XU H. A remote sensing index for assessment of regional ecological changes. *China Environmental Science*, **33** (5), 889, **2013**.
32. WU Z., WANG M., CHEN S., ZOU D. Monitoring and evaluation of ecological environments spatio-temporal variation in mine based on RSEI a case of Yongding mine. *Ecologic Science*, **35** (5), 200, **2016**.
33. JIANG C.L., WU L., LIU D., WANG S.M. Dynamic monitoring of eco-environmental quality in arid desert area by remote sensing: Taking the Gurbantunggut Desert China as an example. *Ying yong sheng tai xue bao*, **30** (3), 877, **2019**.
34. SONG H.M., XUE L. Dynamic monitoring and analysis of ecological environment in Weinan City, Northwest China based on RSEI model. *Ying yong sheng tai xue bao*, **27** (12), 3913, **2016**.
35. WANG S., ZHANG X., ZHU T., YANG W., ZHAO J. Assessment of ecological environment quality in the Changbai Mountain Nature Reserve based on remote sensing technology. *Progress in Geography*, **35** (10), 1269, **2016**.
36. HAN F., YANG Z., SHI H., LIU Q., WALL G. How to Promote Sustainable Relationships between Heritage Conservation and Community, Based on a Survey. *Sustainability*, **8** (9), 886, **2016**.
37. SHI H., YANG Z., HAN F., SHI T., LUAN F. Characteristics of temporal-spatial differences in landscape ecological security and the driving mechanism in Tianshi scenic zone of Xinjiang. *Progress in Geography*, **32** (3), 475, **2013**.
38. LI D., YOU Y.N., LUAN F.M., CHEN X.G. A research of tourism landscape resources evaluation and protection for Bogda World Natural Heritage Site. *World Regional Studies*, (01), 159, **2015**.
39. ZHEN Y., SUN W., GUO X.C., LIANG T., GAO J.G., ZHOU H.R. Structural characteristic and orogenic mechanism of Bogeda Tectonic Belt, Xinjiang. *Journal of East China Institute of Technology*, (02), 199, **2014**.
40. WANG Z., DU X. Monitoring Natural World Heritage Sites: optimization of the monitoring system in Bogda with GIS-based multi-criteria decision analysis. *Environmental Monitoring and Assessment*, **188** (7), 384, **2016**.
41. HA S., YANG Z. Suitability Assessment of the Tools Under a Three-Dimension System of Landscape Monitoring: A Case Study in the NWHS of Bogda. *Sustainability*, **12** (2), 649, **2020**.
42. LIU Q., YANG Z., SHI H., WANG Z. Ecological risk assessment of geohazards in Natural World Heritage Sites: an empirical analysis of Bogda, Tianshan. *Open Geosciences*, **11** (1), 327, **2019**.
43. TUMUR A., MAMUT R., ABBAS A. Community structure characteristics of saxicolous lichens in the Bogda Mountains of Xinjiang, China. *Acta Ecologica Sinica*, **38** (3), 1053, **2018**.
44. JI X., LUO L., WANG X., LI L., WAN H. Identification and Change Analysis of Mountain Altitudinal Zone in Tianshan Bogda Natural Heritage Site Based on DEM-NDVI-Land Cover Classification. *Journal of Geo-Information Science*, **20** (9), 1350, **2018**.
45. HE Y., YANG T. Climate variation and glacier response in the Bogda region, Tianshan Mountains. *Progress in Geography*, **33** (10), 1387, **2014**.
46. LIU P., REN C.Y., WANG Z.M., ZHANG B., CHEN L. Assessment of the eco-environmental quality in the Nanweng River Nature Reserve, Northeast China by remote sensing. *Ying yong sheng tai xue bao*, **29** (10), 3347, **2018**.
47. GUO Z., WEI W., PANG S., LI Z., ZHOU J., XIE B. Spatio-Temporal evolution and motivation analysis of

- ecological vulnerability in Arid Inland River Basin based on SPCA and remote sensing index: A case study on the Shiyang River Basin. *Acta Ecologica Sinica*, **39** (7), 2558, **2019**.
48. XIAN P.W., SHUN Y.U., DA T. The Heritage Value of Mountain Vertical Zonation in Temperate Desert Region of China. *Arid Zone Research*, **26** (5), 694, **2009**.
 49. SHAN W., JIN X., REN J., WANG Y., XU Z., FAN Y., GU Z., HONG C., LIN J., ZHOU Y. Ecological environment quality assessment based on remote sensing data for land consolidation. *Journal of Cleaner Production*, 239, **2019**.
 50. DE KEERSMAECKER W., LHERMITTE S., HONNAY O., FARIFTEH J., SOMERS B., COPPIN P. How to measure ecosystem stability? An evaluation of the reliability of stability metrics based on remote sensing time series across the major global ecosystems. *Global Change Biology*, **20** (7), 2149, **2014**.
 51. WANG B., DING M., GUAN Q., AI J. Gridded assessment of eco-environmental vulnerability in Nanchang city. *Acta Ecologica Sinica*, **39** (15), 5460, **2019**.
 52. LIU Z., XU H., LI L., TANG F., LIN Z. Ecological Change in the Hangzhou Area Using the Remote Sensing Based Ecological Index. *Journal of Basic Science and Engineering*, **23** (4), 728, **2015**.
 53. SONG M., LUO Y., DUAN L. Evaluation of Ecological Environment in the Xilin Gol Steppe Based on Modified Remote Sensing Ecological Index Model. *Arid Zone Research*, **36** (6), 1521, **2019**.
 54. ZHANG Y., ZHANG X., CAI H. Temporal and Spatial Evolutions and Its Driving Factors of Ecological Vulnerability in Wan'an County of Jiangxi Province Based on Geodetector. *Bulletin of Soil and Water Conservation*, **38** (4), 207, **2018**.
 55. SHAN W., JIN X., MENG X., YANG X., XU Z., GU Z., ZHOU Y. Dynamical monitoring of ecological environment quality of land consolidation based on multi-source remote sensing data. *Transactions of the Chinese Society of Agricultural Engineering*, **35** (1), 234, **2019**.
 56. WRIGHT C.K., DE B.K.M., HENEUBRY G.M. Combined analysis of land cover change and NDVI trends in the Northern Eurasian grain belt. *Frontiers of Earth Science*, **6** (2), 177, **2012**.
 57. ZHOU M., CAI Y., ZHANG R., LIU J., SONG X. The tempo-spatial pattern of regional ecological vulnerability before and after the establishment of National Nature Reserve in Helan Mountain of Ningxia. *Ecologic Science*, **38** (5), 78, **2019**.
 58. BAIG M.H.A., ZHANG L., SHUAI T., TONG Q. Derivation of a tasseled cap transformation based on Landsat 8 at-satellite reflectance. *Remote Sensing Letters*, **5** (5), 423, **2014**.
 59. CRIST E.P. A TM tasseled cap equivalent transformation for reflectance factor data. *Remote Sensing of Environment*, **17** (3), 301, **1985**.
 60. IMHOFF M.L., ZHANG P., WOLFE R.E., BOUNOUA L. Remote sensing of the urban heat island effect across biomes in the continental USA. *Remote Sensing of Environment*, **114** (3), 504, **2010**.
 61. SANDHOLT I., RASMUSSEN K., ANDERSEN J. A simple interpretation of the surface temperature/vegetation index space for assessment of surface moisture status. *Remote Sensing of Environment*, **79** (2-3), 213, **2002**.
 62. LIN J., HU G., QI X., XU C., ZHANG A., CHEN W., SHUAI C., LIANG C. Ecological environmental vulnerability and its driving forces in urban agglomeration in the Fujian Delta region. *Acta Ecologica Sinica*, **38** (12), 4155, **2018**.
 63. ZHANG X., LIU X., ZHAO Z., MA Y., YANG Y. Dynamic monitoring of ecology and environment in the agro-pastoral ecotone based on remote sensing: a case of Yanchi County in Ningxia Hui Autonomous Region. *Arid Land Geography*, **40** (5), 1070, **2017**.
 64. LI N., LI T., FANG Y., ZHOU L., WANG Y., ZHAO W. Spatiotemporal Pattern Evolution of Economic Efficiency in County Area of Jilin Province Based on Malmquist and ESDA. *Scientia Geographica Sinica*, **39** (8), 1293, **2019**.
 65. WANG B., ZHANG X. The Contribution of Highway Traffic Infrastructure Construction to Economic Growth in Xinjiang Based on I-O and ESDA. *Acta Geographica Sinica*, **65** (12), 1522, **2010**.
 66. WANG J., ZHANG X., DU H. Spatial Pattern Evolvement and Characteristics of the Economy in Xinjiang at the County Level. *Progress in Geography*, **30** (4), 470, **2011**.
 67. WANG J., XU C. Geodetector: Principle and prospective. *Acta Geographica Sinica*, **72** (1), 116, **2017**.
 68. YU G., LI J., SUN J., SHEN P., YANG C.B. Research on BMI influencing factors of urban male adolescents in China based on geographical detector. *Geographical Research*, **38** (9), 2288, **2019**.
 69. PENG W., ZHANG D., LUO Y., TAO S., XU X. Influence of natural factors on vegetation NDVI using geographical detection in Sichuan Province. *Acta Geographica Sinica*, **74** (9), 1758, **2019**.
 70. TIAN M., YAN C., ZHOU J. Influence of varying cover-soil thickness on the restoration of degraded riparian grassland. *Pratacultural Science*, **36** (9), 2193, **2019**.
 71. ANWAR T., ABDULLA A. Saxicolous Lichen Species Diversity in Bogda Mountains, Xinjiang. *Journal of North-East Forestry University*, **45** (11), 60, **2017**.
 72. LOUHAICHI M., BELGACEM A.O., PETERSEN S.L., HASSAN S. Effects of climate change and grazing pressure on shrub communities of West Asian rangelands. *International Journal of Climate Change Strategies and Management*, **11** (5), 660, **2019**.
 73. RUAN, W., LI Y., ZHANG S., LIU C.H. Evaluation and drive mechanism of tourism ecological security based on the DPSIR-DEA model. *Tourism Management*, **75**, 609, **2019**.
 74. GULJIANG H.Z., LIANG Y. Forest fire prevention and control measures in Xinjiang Tianchi Bogedafeng Nature Reserve. *Forest Fire Prevention*, (02), 8, **2019**.
 75. TANG X.B. A survey of Tianchi Scenic Spot in Xinjiang based on tourist satisfaction. *Science & Technology Vision*, (12), 39, **2012**.
 76. NIU S.M., LIANG Y., ZHANG S.L. Forest Fire prevention and control measures after banning grazing in Xinjiang Tianchi Nature Reserve. *Forest Fire Prevention*, (01), 30, **2015**.
 77. BOURGOIN C., OSZWALD J., BOURGOIN J., GOND V., BLANC L., DESSARD H., TRONG V.P., SIST P., LADERACH P., REYMONDIN L. Assessing the ecological vulnerability of forest landscape to agricultural frontier expansion in the Central Highlands of Vietnam. *International Journal of Applied Earth Observation and Geoinformation*, **84**, **2020**.
 78. NIU S.M., LI Z.Q., HUAI B.J. Glaciers changes in Bogeda region, Tianshan in the last 50 years. *Journal of Arid Land Resources and Environment*, (09), 134, **2014**.
 79. WANG P., LI Z., LI H., WU L., JIN S., ZHOU P. Changes of Ice-thickness and Volume for Representative Glaciers

- in Tianshan Mountains in the Past 50 Years. *Acta Geographica Sinica*, **67** (7), 929, **2012**.
80. WANG R., ZHAO G., ZHOU W., ZHU X., WANG J., QIN Y. Assessment of the impacts of land use on regional ecological environmental vulnerability. *Transactions of the Chinese Society of Agricultural Engineering*, **24** (12), 215, **2008**.
 81. SHI D., LIANG Y. Evaluation and Conservation of Fragile Ecological Environment in China. *Journal of soil and water conservation*, **16** (1), 6, **2002**.
 82. CHEN W., XIAO D., LI X. Classification, application, and creation of landscape indices. *The Journal of Applied Ecology*, **13** (1), 121, **2002**.
 83. NIU J. Impacts Prediction of Climatic Change on Distribution and Production of Grassland in Inner Mongolia. *Acta Agrestia Sinica*, **9** (4), 277, **2001**.
 84. IONESCU C., KLEIN R.J.T., HINKEL J., KUMAR K.S.K., KLEIN, R. Towards a Formal Framework of Vulnerability to Climate Change. *Environmental Modeling & Assessment*, **14** (1), 1, **2009**.
 85. SHI H., YANG Z., HAN F., LUAN F., SHI T. Assessment and analysis of eco-environment vulnerability in Tomur region of natural heritage site. *Arid Land Geography*, **36** (2), 318, **2013**.
 86. HA K., DING Q., MEN M., XU H. Spatial distribution of land use and its relationship with terrain factors in hilly area. *Geographical Research*, **34** (5), 909, **2015**.
 87. HOBBS R.J., SAUNDERS D.A., ARNOLD G.W. Integrated landscape ecology - a western -australian perspective. *Biological Conservation*, **64** (3), 231, **1993**.
 88. DONG S., ZHAO Y., LI X. Spatiotemporal Patterns of Land Use Change in Plateau Region Based on the Terrain Gradient -A Case Study in Panxian County,Guizhou Province. *Research of Soil and Water Conservation*, **24** (2), 213, **2017**.
 89. LI F., CHANG Q., SHEN J., LIU J. Dynamic monitoring of ecological environment in loess hilly and gully region of Loess Plateau based on remote sensing: A case study on Fuxian County in Shaanxi Province. Northwest China. *Ying yong sheng tai xue bao*, **26** (12), 3811, **2015**.
 90. YUE H., LIU Y., ZHU R. Monitoring Ecological Environment Change Based on Remote Sensing Ecological Index in Shendong Mining Area. *Bulletin of Soil and Water Conservation*, **39** (2), 101, **2019**.
 91. WOLTERS M.L., SUN Z., HUANG C., KUENZER C. Environmental awareness and vulnerability in the Yellow River Delta: Results based on a comprehensive household survey. *Ocean & Coastal Management*, **120**, 1, **2016**.
 92. LI L., SHI Z.H., YIN W., ZHU D., NG S.L., CAI C.F., LEI A.L. A fuzzy analytic hierarchy process (FAHP) approach to eco-environmental vulnerability assessment for the danjiangkou reservoir area, China. *Ecological Modelling*, **220** (23), 3439, **2009**.